

KDAR neutrino scattering for ^{12}C target via charged current and muon angular distribution

Chaeyun Lee ^{*},¹ Kyungsik Kim [†],² Myung-Ki Cheoun [‡],¹
Eunja Ha [§],³ Tatsushi Shima [¶],⁴ and Toshitaka Kajino ^{**}⁵

¹*Department of Physics and OMEG Institute,
Soongsil University, Seoul 06978, Korea*

²*School of Liberal Arts and Science,
Korea Aerospace University, Koyang 412-791, Korea*

³*Department of Physics and Research Institute for Natural Science,
Hanyang University, Seoul, 04763, Korea*

⁴*Research Center for Nuclear Physics,
Osaka University, Osaka 567-0047, Japan*

⁵*School of Physics and International Research Center
for Big-Bang Cosmology and Element Genesis,
Beihang University, Beijing 100083, China,
The University of Tokyo, 7-3-1 Hongo,
Bunkyo-ku, Tokyo 113-0033, Japan,*

National Astronomical Observatory of Japan 2-21-1 Osawa, Mitaka, Tokyo 181-8588, Japan

(Dated: September 4, 2024)

* e-mail: cylee31005@gmail.com

† e-mail: kyungsik@kau.ac.kr

‡ e-mail: cheoun@ssu.ac.kr (Corresponding Author)

§ e-mail: ejaha@hanyang.ac.kr

¶ e-mail: shima@rcnp.osaka-u.ac.jp

** e-mail: kajino@buaa.edu.cn

Abstract

We calculate muon-neutrino (ν_μ) scattering off ^{12}C via charged current (CC) by exploiting the 236 MeV ν_μ from the kaon-decay-at-rest (KDAR). In this energy region, since both inelastic scattering below the quasielastic (QE) region and the QE scattering contribute simultaneously, we combine the inelastic scattering obtained by the QRPA and the QE scattering obtained by distorted wave born approximation (DWBA) based on the relativistic mean field (RMF) theory. We compare the results to the data from MiniBooNE. Further, since the KDR ν_μ CC scattering may have angle dependence of outgoing muon, we investigate the differential angular dependent cross section in the ν_μ - ^{12}C scattering and compare to the results by ν_e - ^{12}C scattering. These results could be useful for the calibration of the forthcoming KDAR neutrino cross section experiments.

I. INTRODUCTION

Neutrino (ν) (antineutrino ($\bar{\nu}$))-induced reactions on complex nuclei play important roles on understanding not only the nuclear structure probed by the weak interaction [1–7], but also exploring some key ν -parameters relevant to the ν -physics [8, 9]. For example, neutrino mass hierarchy, matter effects of ν -oscillation, ν -self interaction as well as the information of the matter contents may be constrained through detailed analysis of nuclear abundances in core collapsing supernova (SN) explosions [9–11]. Recently, much interest has been focused on the neutrino (ν)-process [8–13] for medium and medium-heavy nuclei as well as light elements because emitted neutrino flux is expected to be sufficiently high enough to produce some specific nuclei blocked by β -decay due to the surrounding stable seed nuclei, in spite of small cross sections of the weak interaction. Therefore, cross sections for neutrino (antineutrino)-nucleus ($\nu(\bar{\nu})-A$) reactions are to be treated as important input data for network calculations estimating relevant nuclear abundances, in specific, for the weak rapid process [14–16]. Not only for the nucleosynthesis, but also for the analysis of recent accelerator-based and reactor-based neutrino experiments one needs also detailed understanding of the relevant neutrino-nucleus cross section [17].

Since most neutrinos for these experiments are usually produced via decay-in-flight (DIF) and three-body beta decay of the pions and/or kaons created in proton-nucleus scattering, they have a broad range of energies, which causes a major stumbling block and needs the reconstruction of the incident neutrino energy with a specific model in the experimental analysis. In addition to the issues associated with the reconstruction of the neutrino energy, the precise evaluation of the underlying nuclear response functions to the electro-weak interaction gives rise to some nuclear model dependence on the interpretation of the experimental observables due to the shortage of the weak-interacting nuclear structure as well as their feeble cross sections.

Kaon-decays-at-rest (KDAR) neutrinos offer an optimized opportunity to study neutrino-nucleus interactions without the broad energy complications raised by the neutrinos coming from meson decay-in-flight (DIF). Besides the important study of the sterile neutrino study by the KDAR neutrino [18–20], these mono-energetic 236-MeV ν_μ beam presents an excellent tool for more unambiguous calibration of cross sections and the determination of weak-interaction parameters inside nuclei. Therefore, KDAR ν_μ could be very useful for reducing

experimental and theoretical uncertainties and ambiguities in an unprecedented way.

KDAR neutrinos are also very useful for understanding astrophysical neutrinos because the neutrino sources produced by high energy proton accelerators through the meson DIF amount to GeV-scale producing too high energy to study the supernova neutrino thought to be located in tens of MeV region. Further, the neutrino interactions with nuclei in this energy region are rarely known apart from a few data from those of laboratory-made neutrinos like LSND [20] and KARMEN [21–23].

Therefore, owing to their relatively small energy, the 236 MeV KDAR ν_μ provides an important opportunity to gain insight into the interactions of the core collapsing supernova and their neutrino processes [10, 11] as well as the sterile neutrino study [24, 25]. KDAR ν_μ provides cross sections with energy transfers up to $E_\nu - m_\mu \sim 130$ MeV thereby covering a range of nuclear responses that complies with the realm of supernova neutrinos. In particular, forward scattering of 236 MeV ν_μ with low-momentum transfers should be able to provide precious information about the low-energy excitations important in the interactions of astrophysical neutrinos, complementing experiments performed with the neutrinos from muon decay-at-rest at lower energy around $E_{\nu_\mu} = 30$ MeV region [26–31].

However, the ν - A scattering in the energy region has the contribution from the two-step process (inelastic scattering) as well as one-step process (QE scattering) [32]. For the two-step process, the incident neutrino directly excites target nucleus, and then the excited target nucleus is subsequently decayed into other nuclei by emitting some particles incoherently. The excitation occurs through various multipole transitions i.e., super allowed Fermi ($J^\pi = 0^+$), allowed Gamow-Teller ($J^\pi = 1^+$), spin dipole ($J^\pi = 0^-, 1^-, 2^-$), and other higher multipole transitions. Therefore dominant contributions of the two-step process stem from discrete and giant resonance (GR) states of the compound nucleus. Their typical excitation energies amount to tens of MeV. But, the one-step process is also possible, in which a nucleon inside a target nucleus is directly knocked out from the target nucleus due to sufficient momentum transfer without any significant excitation of target nucleus. Indeed, the one-step process is the main reaction in the quasi-elastic (QE) peak region, where the incident neutrino scatters off individual nucleons quasi-freely. If the outgoing particles in the two-step process are nucleons, both processes could not be distinguished in the experimental measurement because these two processes have identical final states. For example, $^{12}\text{C}(\nu, \nu')$ $^{12}\text{C}^* \rightarrow ^{11}\text{B} + \text{p}$ (or $^{11}\text{C} + \text{n}$) reaction via NC could not be distinguished from $^{12}\text{C}(\nu, \nu' p)^{11}\text{B}$

(or $^{12}\text{C}(\nu, \nu' n)^{11}\text{C}$). Similarly, $^{12}\text{C}(\nu_e, e^-)^{12}\text{N}^* \rightarrow ^{11}\text{C} + \text{p}$ and $^{12}\text{C}(\bar{\nu}_e, e^+)^{12}\text{B}^* \rightarrow ^{11}\text{B} + \text{n}$ reactions through CC also could not be differentiated, respectively, from $^{12}\text{C}(\nu_e, e^- p)^{11}\text{C}$ and $^{12}\text{C}(\bar{\nu}_e, e^+ n)^{11}\text{B}$.

Experimentally, the KDAR neutrino has begun to be studied, although there are now a number of existing and planned experiments that will be able to take advantage of it. As one example, the NuMI beamline absorber at Fermilab is a prominent KDAR ν_μ source. A number of neutrino detectors in the vicinity of the NuMI beam absorber are sensitive to these neutrinos. Recently, MiniBooNE, a Cherenkov- and scintillation-based mineral oil detector located about 85 m from the NuMI beamline absorber, has successfully isolated 236-MeV KDAR ν_μ events using muon energy reconstruction and timing information [25]. Thereby, the MiniBooNE collaboration reported the first (and only so far) measurement of monoenergetic KDAR ν_μ interactions on ^{12}C [25]. Recent progress of the J-PARC Sterile Neutrino Search at the J-PARC Spallation Neutron Source (JSNS²) project which uses the 3 GeV pulsed proton beam is also prominent facility for producing the KDAR neutrino [18, 19].

In this work, we study total and differential cross section for charged current quasielastic (CCQE) and inelastic scattering by 236-MeV KDAR neutrinos. Importantly, the relevant energy transfer for these interactions is situated at the low-energy part of the genuine quasielastic region. The impact of nuclear effects and low-energy excitations can therefore be expected to be relatively large, which needs a detailed microscopic modelling of these neutrino reactions, with a careful treatment of nuclear physics effects, mandatory [33]. To describe the low-energy ν -interaction with nuclei and the QE scattering, we exploit, respectively, the quasi-particle-random-phase-approximation (QRPA) model for the inelastic scattering and some relativistic mean field (RMF) models in the DWBA framework for QE scattering. Further, the outgoing muon may have angle dependence by the momentum transfer, which may provide more meaningful informations for the weak-nuclear structure. We estimate the angular distribution of outgoing lepton with the detailed analysis of the contribution of each multipole transition.

II. THEORETICAL FRAMEWORK

By using the weak current operator, which is composed of longitudinal ($\hat{\mathcal{L}}_J$), Coulomb ($\hat{\mathcal{M}}_J$), electric ($\hat{\mathcal{T}}_J^{el}$) and magnetic operators ($\hat{\mathcal{T}}_J^{mag}$) detailed at Ref.[34], we calculate the differential cross section for $\nu(\bar{\nu})$ - ^{12}C reactions as follows [35–37]

$$\begin{aligned}
\left(\frac{d\sigma_\nu}{d\Omega}\right)_{(\nu/\bar{\nu})} &= \frac{G_F^2 \epsilon k}{\pi (2J_i + 1)} \left[\sum_{J=0} (1 + \vec{\nu} \cdot \vec{\beta}) | \langle J_f | \hat{\mathcal{M}}_J | J_i \rangle |^2 \right. \\
&+ (1 - \vec{\nu} \cdot \vec{\beta} + 2(\hat{\nu} \cdot \hat{q})(\hat{q} \cdot \vec{\beta})) | \langle J_f | \hat{\mathcal{L}}_J | J_i \rangle |^2 - \\
&\hat{q} \cdot (\hat{\nu} + \vec{\beta}) 2\text{Re} \langle J_f | \hat{\mathcal{L}}_J | J_i \rangle \langle J_f | \hat{\mathcal{M}}_J | J_i \rangle^* \\
&+ \sum_{J=1} (1 - (\hat{\nu} \cdot \hat{q})(\hat{q} \cdot \vec{\beta})) (| \langle J_f | \hat{\mathcal{T}}_J^{el} | J_i \rangle |^2 + | \langle J_f | \hat{\mathcal{T}}_J^{mag} | J_i \rangle |^2) \\
&\left. \pm \sum_{J=1} \hat{q} \cdot (\hat{\nu} - \vec{\beta}) 2\text{Re} [\langle J_f | \hat{\mathcal{T}}_J^{mag} | J_i \rangle \langle J_f | \hat{\mathcal{T}}_J^{el} | J_i \rangle^*] \right], \tag{1}
\end{aligned}$$

where (\pm) stems from the different helicities of $\nu(\bar{\nu})$, respectively. $\vec{\nu}$ and \vec{k} are incident and final lepton 3-momenta, $\vec{q} = \vec{k} - \vec{\nu}$ and $\vec{\beta} = \vec{k}/\epsilon$ with the final lepton's energy ϵ . The nuclear matrix elements of the weak interaction Hamiltonian can be expanded in terms of multipole operators by using two basic operators

$$M_J^{M_J}(q\mathbf{x}) = j_J(qx) Y_J^{M_J}(\Omega_x), \quad \mathbf{M}_{JL}^{M_J}(q\mathbf{x}) = j_J(qx) \mathbf{Y}_{JL1}^{M_J}(\Omega_x), \tag{2}$$

where vectorial spherical harmonic $\mathbf{Y}_{JL1}^{M_J}(\Omega_x)$ is expressed in term of spherical harmonic $Y_L^m(\Omega_x)$, *i.e.* $\mathbf{Y}_{JL1}^{M_J}(\Omega_x) = \sum_{m\lambda} \langle Lm1\lambda | (L1)JM_J \rangle Y_L^m(\Omega_x) \mathbf{e}_\lambda$. Then we rewrite any one-body transition matrix element $\hat{\mathcal{O}}_{JM;TM_T}^{(1)}(q\mathbf{x})$ in terms of the 4 different transition operator (Coulomb, longitudinal, electric and magnetic) as follows

$$\begin{aligned}
\hat{\mathcal{M}}_{JM;TM_T}(q\mathbf{x}) &= [F_1^{(T)} M_J^{M_J}(q\mathbf{x}) - i \frac{q}{M} [F_A^{(T)} \Omega_J^{M_J}(q\mathbf{x}) + \frac{F_A - \omega F_P^{(T)}}{2} \Sigma_J''^{M_J}(q\mathbf{x})]] I_T^{M_T}, \tag{3} \\
\hat{\mathcal{L}}_{JM;TM_T}(q\mathbf{x}) &= \left[\frac{-\omega}{q} F_1^{(T)} M_J^{M_J}(q\mathbf{x}) + i (F_A^{(T)} - \frac{q^2}{2M_N} F_P^{(T)}) \Sigma_J''^{M_J}(q\mathbf{x}) \right] I_T^{M_T}, \\
\hat{\mathcal{T}}_{JM;TM_T}^{el}(q\mathbf{x}) &= \left[\frac{q}{M} [F_1^{(T)} \Delta_J'^{M_J}(q\mathbf{x}) + \frac{1}{2} \mu^{(T)} \Sigma_J^{M_J}(q\mathbf{x})] + i F_A^{(T)} \Sigma_J'^{M_J}(q\mathbf{x}) \right] I_T^{M_T}, \\
\hat{\mathcal{T}}_{JM;TM_T}^{mag}(q\mathbf{x}) &= -i \frac{q}{M} \left[[F_1^{(T)} \Delta_J^{M_J}(q\mathbf{x}) - \frac{1}{2} \mu^{(T)} \Sigma_J'^{M_J}(q\mathbf{x})] + F_A^{(T)} \Sigma_J^{M_J}(q\mathbf{x}) \right] I_T^{M_T},
\end{aligned}$$

where the 7 relevant single particle operators ($M_J^{M_J}, \Omega_J^{M_J}, \Sigma_J''^{M_J}, \Delta_J^{M_J}, \Sigma_J^{M_J}, \Sigma_J'^{M_J}, \Delta_J'^{M_J}$) are detailed at Refs.[36, 38]. The superscript $T(= 0, 1)$ means isoscalar and isovector. $I_T^{M_T}$ stands for the isospin dependence [36]. Single nucleon form factors $F_X^{(T)}(Q^2)$ with $T = 0, 1$ and $X = 1, 2, S, A, P, T$ are Dirac ($X = 1$), Pauli ($X = 2$), scalar, axial, pseudo-scalar, and

tensor form factors, respectively. Detailed form factors are referred from Ref. [36, 38], and we take F_S and F_T to be zero because of current conservation and no existence of second class current, respectively. Here we note that these operators include the GT and Fermi transitions including the forbidden parts as well as other spin dipole resonance transitions. The multipole transitions are calculated by the QRPA framework [39], whose results turned out to agree with the SM calculation [3, 12].

For CC reactions we multiplied Cabbibo angle $\cos^2\theta_c$ and considered the Coulomb distortion of outgoing leptons in a residual nucleus [3, 12, 43]. By following the prescriptions adopted in Refs.[43, 45], we choose an energy point in which both approaches predict same values. Then we use the Fermi function below the energy and the effective momentum approach (EMA) above the energy [40–42].

This cross section can be reduced to the following simple total cross section, by putting the 3-momentum of the outgoing lepton $\vec{k} = 0$ and considering the Fermi and the GT transitions

$$\sigma(E_\nu) = \frac{G_F^2 \cos^2\theta_c}{\pi \hbar^4 c^3} k \epsilon F(Z, \epsilon_i) [B(GT) + B(F)] , \quad (4)$$

where k and ϵ refer to momentum and total energy of the outgoing lepton and $F(Z, \epsilon_i)$ accounts for the Coulomb correction. The GT and Fermi strength distribution, $B(GT)$ and $B(F)$, are given as follows

$$B(GT\pm) = \frac{g_A^2}{2J_i + 1} \sum_{M_i, M_f} | \langle J_f, M_f | \sum_{k=1}^A \tau_{\pm} \sigma | J_i, M_i \rangle |^2 , \quad (5)$$

$$B(F\pm) = \frac{g_V^2}{2J_i + 1} \sum_{M_i, M_f} | \langle J_f, M_f | \sum_{k=1}^A \tau_{\pm} | J_i, M_i \rangle |^2 .$$

Since Eq.(4) is valid only near threshold of the outgoing lepton as commented at Ref. [61], it may not be applied for the incident neutrino energy beyond the lepton threshold considered in this report. Even for solar neutrinos, the contributions by other multipole transitions may become significant.

Here we make a note on the meaning of the 1^+ transition exploited in the neutrino cross section in Eq.(2), which is used differently from the allowed GT(1^+) transition for the β -decay or charge exchange reactions. For neutrino-induced reaction cross sections, we include the forbidden 1^+ transitions as well as the allowed GT transition, while only the allowed GT transition is usually considered at the GT strength distributions. Hereafter, we denote the

corresponding 1^+ transition for neutrino reaction as 1^+ transition to distinguish the allowed GT transition. Of course, the 1^+ transition is reduced to the allowed GT transition at the threshold limit. It means that the Ikeda sum rule (ISR) useful for the GT transition may not hold in the ν and $\bar{\nu}$ cross sections. For the neutrino-induced reactions, we did not use the quenching factor for any multipole transitions because the ISR for the GT transition is more or less satisfied and we do not know the quenching factors for other multipole transitions.

For the QE region we exploit the RMF model, which has been briefly introduced in the following. The quantum hadrodynamics (QHD), as a representative RMF nuclear model, has been established by Walecka within a relativistic framework for describing nuclear many-body system, where the point like nucleons interact through the exchange of scalar (σ) and vector (ω) meson [46]. This model has achieved great success in understanding the saturation mechanism of infinite matter and the characteristics of doubly magic nuclei with the inclusion of isovector (ρ) meson [47]. Boguta and Bodmer introduced a nonlinear σ self-coupling, the so-called nonlinear σ (NL) model [48], to reproduce the realistic nuclear incompressibility because the equation of state (EoS) given by the naive QHD was too hard. The NL has been used to describe not only light doubly magic nuclei but heavy deformed nuclei [49, 50]. Guichon [51] propose the quark-meson coupling (QMC) model, in which the properties of nuclear matter can be self-consistently calculated by the coupling of meson fields to the quarks within the nucleons rather than to the nucleons themselves [52]. In addition, the QMC model has been extended to include quark-quark hyperfine interactions due to exchanges of gluon and pion based on chiral symmetry [53]. This new version of the chiral QMC (CQMC) model guarantees the conservation of axial vector current in chiral limit, and it was applied to the neutron-star EoS within relativistic Hartree-Fock approximation [54]. Recently the QMC models are extended by including the isovector-scalar δ meson giving rise to the charge symmetry breaking effects and applied to the neutron star physics [55, 56]. These models were successfully applied into the exclusive ($e, e'p$) [57] and inclusive (e, e') [58] reactions for electron-nucleus QE scattering and also shown to be in good agreement with the neutrino QE scattering data [59, 60]. The detail explanations of each models are in Ref. [57].

In this work, we exploit the QRPA model for inelastic scattering and the DWBA model based on the RMF models for describing the KDAR neutrino scattering.

III. RESULTS AND DISCUSSIONS

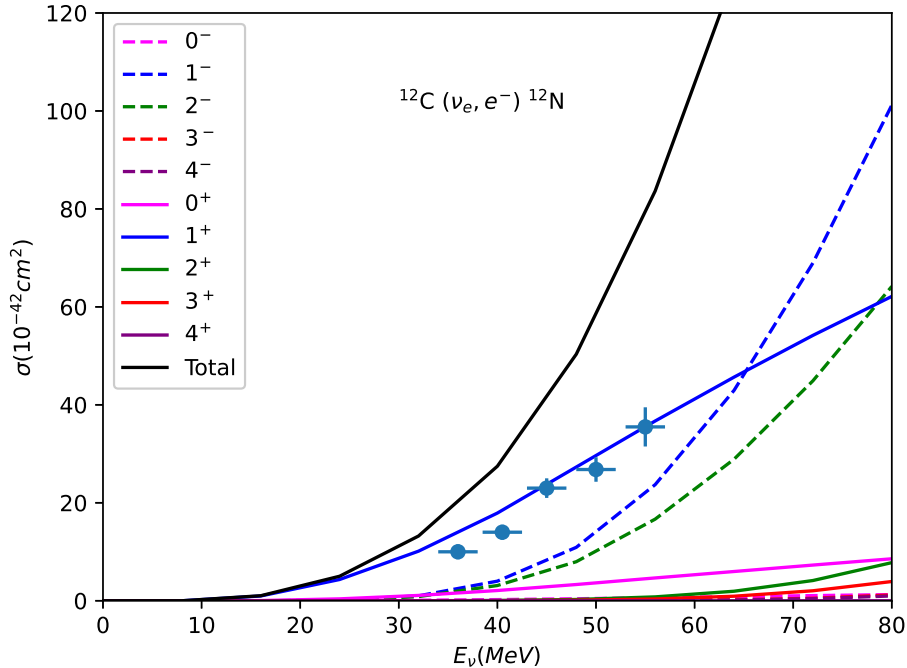


FIG. 1: (Color online) Neutrino-induced cross section via CC for ^{12}C , $^{12}\text{C}(\nu_e, e^-)^{12}\text{N}^*$

A. Cross sections of KDAR neutrino scattering off ^{12}C for muon kinetic energy T_μ

Figure 1 illustrates total cross section of $^{12}\text{C}(\nu_e, e^-)^{12}\text{N}$, which were already provided in previous papers [34, 35] and shown to be consistent with the results by the shell model calculation in Ref.[3]. One point to notice is that the contribution by the 1^+ transition dominates the cross section up to $E_\nu \simeq 60\text{MeV}$. After the region, 1^- spin-dipole (SD) transition becomes dominant with 2^- SD transition.

Before the discussion of the cross section by KDAR ν_μ , in Fig.2, we extend the calculation up to $E_\nu = 300\text{ MeV}$ within the QRPA scheme to study the flavour dependence in the total cross section data. We could not find any significant dependence on neutrino flavour. But interestingly, the main transition is changed to the spin dipole 1^- transition, irrespective of the neutrino flavour, and the muon production threshold energy explicitly appeared.

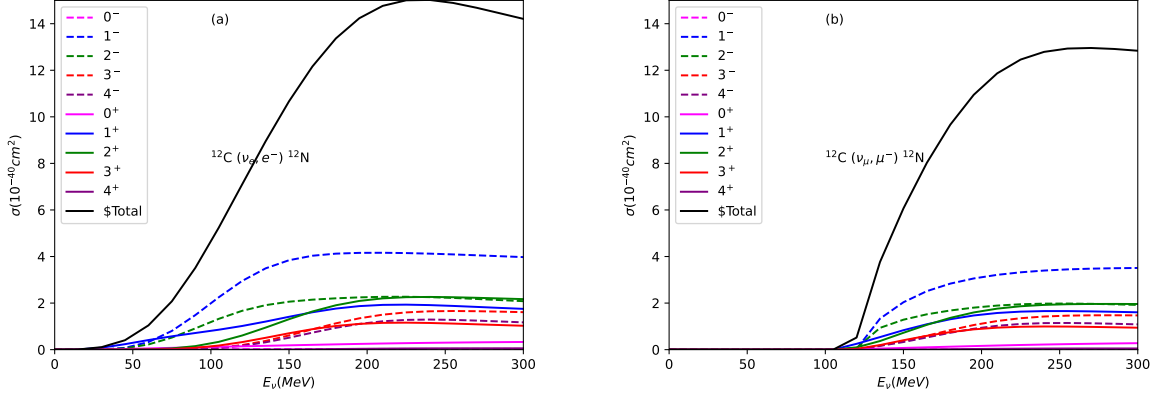


FIG. 2: (Color online) Neutrino-induced cross section via CC (a) for ^{12}C , $^{12}\text{C}(\nu_e, e^-)^{12}\text{N}^*$ and (b) $^{12}\text{C}(\nu_\mu, \mu^-)^{12}\text{N}^*$ upto $E_\nu=300$ MeV

Other spin dipole transition 2^- as well as the 1^+ and 2^+ transitions contribute to some extent to total cross section. Above $E_{\nu_e} \sim 150$ MeV ($E_{\nu_\mu} \sim 250$ MeV), most of the transitions are saturated. It means that the nuclear excitations above the energy region are already exhausted, and the QE scattering becomes dominant above the energy region.

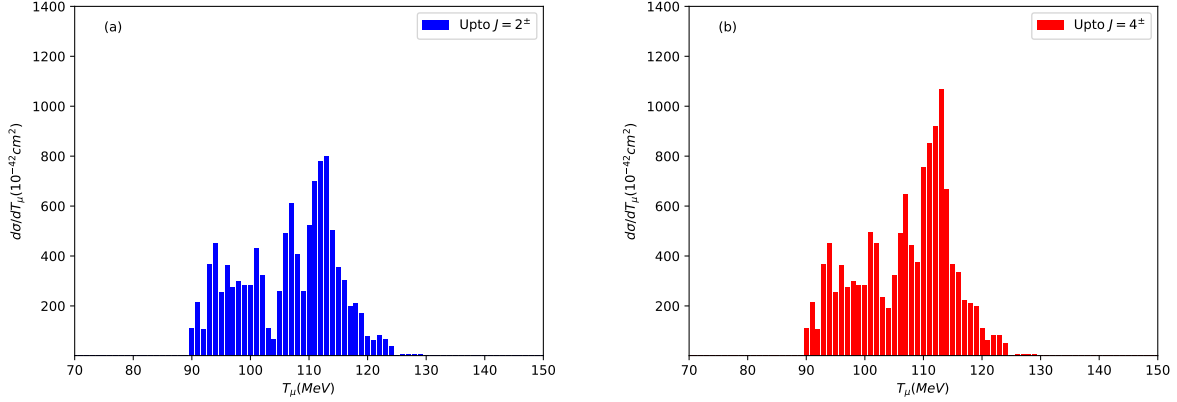


FIG. 3: (Color online) Neutrino cross section via CC for ^{12}C by KDAR neutrino in term of the muon kinetic energy T_{μ} from $J = 0^\pm$ up to (a) $J_{max} = 2^\pm$ and (b) 4^\pm , respectively.

Hereafter, we focus on the differential cross section by KDAR, whose energy is fixed as $E_{\nu_\mu} = 236$ MeV. Figure 3 presents the differential cross section from $J = 0^\pm$ up to $J^\pi = 2^\pm$ and $J^\pi = 4^\pm$. The cross sections are distributed mostly in the region, $90 \text{ MeV} < T_\mu < 125$ MeV, and the most pronounced peaks appear around $E_{\nu_\mu} = 112$ MeV region.

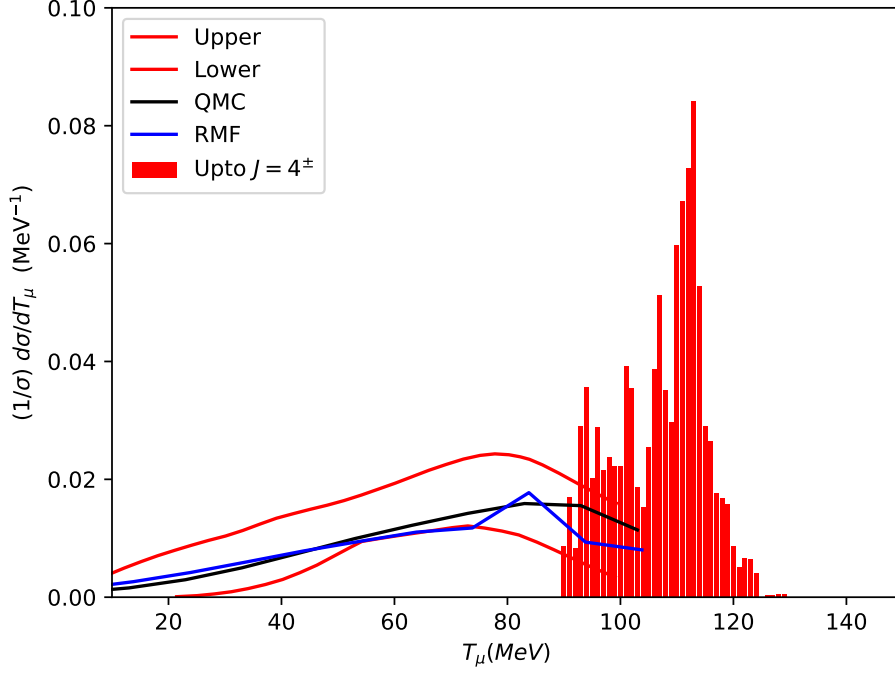


FIG. 4: (Color online) Neutrino cross sections via CC for ^{12}C by KDAR neutrino in the DWBA (blue and black curves) and QRPA (red histograms). They correspond to one-step and two-step processes for the neutrino scattering. The upper and lower red curves show the experimental data by the shape spectrum from MiniBooNE KDAR data [25].

Here we shortly introduce the kinematics used in this work. If we start from the missing energy concept, $E_m = \omega - \sum T_p$, usually used in the electron scattering, $^{12}\text{C}(e, e'p)$, with the energy transfer ω and the outgoing kinetic energy of protons and muons, T_p and T_μ , then the missing energy in the neutrino scattering is given as

$$E_m = \omega - \sum T_p = E_{\nu_\mu} - m_\mu - (T_\mu + \sum T_p). \quad (6)$$

In this work, for inelastic scattering, we assume the missing energy $E_m = 0$ and take total kinetic energy of emitted proton in the inelastic scattering as the nuclear excitation energy, *i.e.* $E^* = \sum T_p$. Then we obtain $E_{\nu_\mu} = m_\mu + T_\mu + E^*$. The cross section in Fig. 3 given by the muon kinetic energy T_μ appears around $T_\mu \simeq 90 \sim 125$ MeV, which means the excitation energy spectra in $E^* = 5 \sim 40$ MeV region are taken into account in the compound nucleus ^{12}N produced by KDAR ν_μ . We also note that about 20% increase obtained by $J^\pi > 2^\pm$ transitions was found in the cross section results.

Figure 4 presents the results by DWBA and QRPA for one-step and two-step process together. The DWBA results are obtained by two different RMF models [59]. One is the simple RMF adopted in Ref. [62] and the other model is the so called QMC model [60] which included the density dependence by the σ meson in the RMF model considering the quark condensation in vacuum, and has been successfully used for neutrino and electron scattering [60].

The cross section denoted as bar graphs in $T_\mu = 90 \sim 125$ MeV (corresponding to $E_{\nu_\mu} = 5 \sim 40$ MeV) are obtained by the QRPA approach, which describes the inelastic scattering taking into account of the excitations in ^{12}N . The cross sections up to $T_\mu = 90$ MeV are obtained by the DWBA considering QE scattering. Here the experimental data are given by the upper and lower curves taken from Ref. [25].

B. Angular distribution of outgoing muon in KDAR scattering

Figure 5 displays the angular distribution of outgoing lepton, respectively, for $E_{\nu_\mu} = 236$ MeV and 180 MeV. They show a clear dependence on the scattered angle of θ_μ . In particular, one can see forward peak around $\theta_\mu = 40^\circ$, whose peak values (positions) increase (shift to forward) with the increase of the incident energy. Main contribution around this angle region stems mainly from the spin dipole transition 1^- and the quadrupole transition 2^- as well as the combination of 1^+ and 2^+ . Interestingly, the GT (1^+) transition take places mainly in the forward direction. If we lower the neutrino energy as $E_{\nu_\mu} = 180$ MeV, the peak position in the panel (b) is shifted a bit to $\theta_\mu = 50^\circ$ region mainly due to the shift by 1^- and 2^+ transition.

However, the situation becomes quite different for the ν_e case. The results for ν_e in Fig.6 show the increase at backward direction, almost irrespective of the incident energy. The difference comes from the lepton mass difference. The heavy lepton (muon) moves to the forward direction, but the lighter electron moves backward in the scattering off the ^{12}C target. Important point for ν_e case is that the main transition contributing to the angular distribution comes from the 1^+ transition in the energy region $E_{\nu_e} < 80$ MeV. But with the increase of incident neutrino energy, the 1^+ transition shifts forward direction while other multipole transitions except 0^+ transition moves still backward direction with the increased contribution. Consequently the angular distribution keeps backward direction. This trend

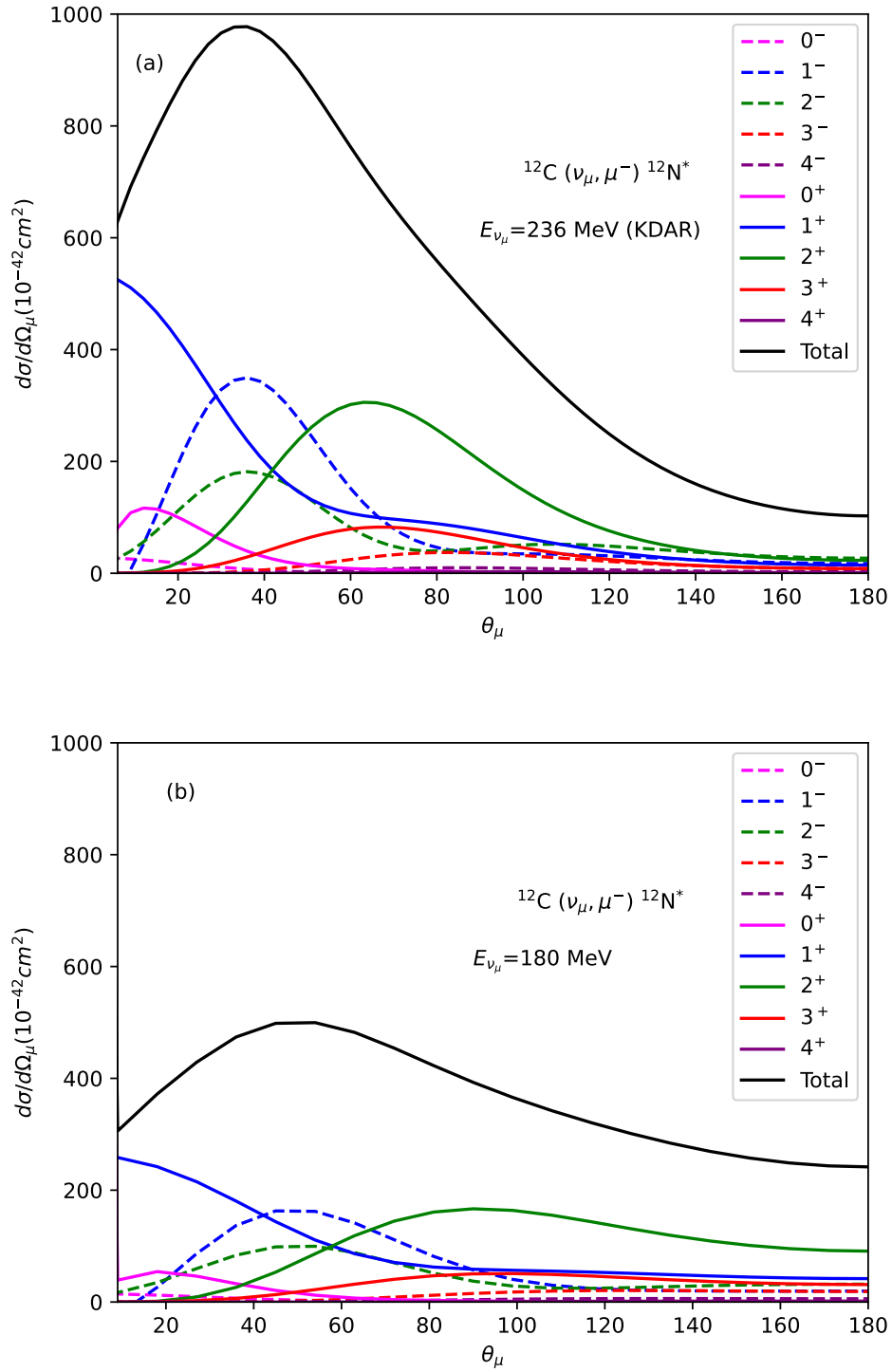


FIG. 5: (Color online) Muon angular distribution cross section via CC (a) for ^{12}C for KDAR neutrino ($E_{\nu_\mu} = 236 \text{ MeV}$) and (b) $E_{\nu_\mu} = 180 \text{ MeV}$ for each $J_{max} = 0^\pm, 1^\pm, 2^\pm, 3^\pm, 4^\pm$, respectively

is quite different from those by ν_μ case in Fig. 5. But it is interesting that the 0^+ transition shows forward direction independent of neutrino flavour.

Another point to deserve notice is that the results for the ν_e case are dominated by the two 1^+ and 0^+ transitions. Above $E_{\nu_e} \simeq 40$ MeV, the spin dipole dominance (1^- and 2^-) appears with backward direction contrary to the ν_μ case. The same spin dipole transition shows different angular distribution tendency depending on the neutrino flavour.

Recent calculation by Fermi gas model with RPA corrections presented backward peaks for both ν_e and ν_μ cases [63]. But the calculation did not include explicitly the multipole transitions. The calculation by CRPA show backward peaks for ν_e scattering for $50 \sim 100$ MeV. This behaviour is compatible with the present calculation. But with the increase of the E_{ν_e} about $300 \sim 500$ MeV, whose energy region is mostly QE scattering region, forward peaks are shown to be prominent for ν_e - ^{16}O scattering [45].

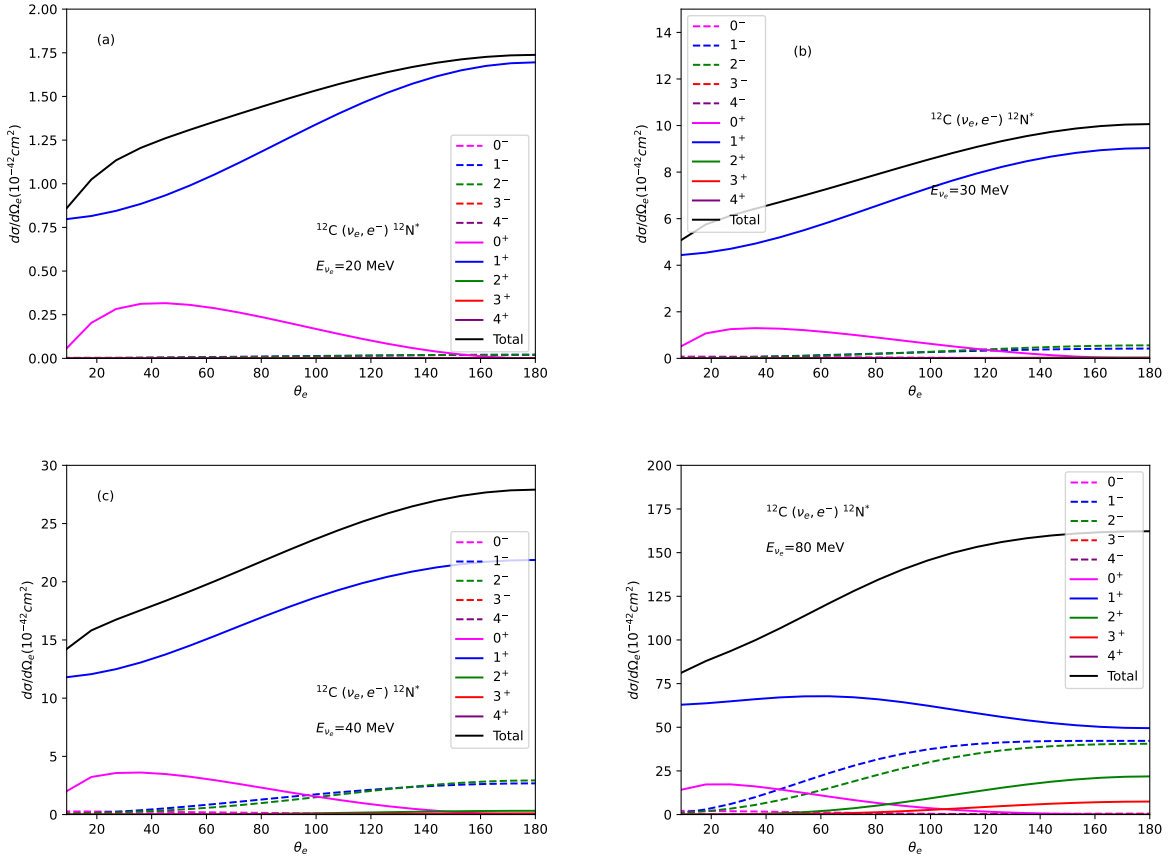


FIG. 6: (Color online) Electron angular distribution cross section for KDAR neutrino via CC for ^{12}C by KDAR neutrino for each $J_{max} = 0^\pm, 1^\pm, 2^\pm, 3^\pm, 4^\pm$, respectively

IV. SUMMARY AND CONCLUSION

First, we calculated the KDAR neutrino scattering off ^{12}C target using the RMF models for QE region and the QRPA for the energy region below the QE region. The QE region data have successfully explained the MiniBooNE data up to around $T_\mu = 100$ MeV region by the RMF approach [59, 60].

Second, but the the cross section in the $T_\mu > 90$ MeV region, the contribution from the inelastic scattering contribute dominates. We added the contribution using the QRPA approach to describe the excitation of the compound nucleus produced by the incident KDAR neutrino. The QRPA calculation has been applied and successfully described the neutrino-induced cross section for various target nuclei expected to be produced in the neutrino-process [10, 11].

Third, since we expect more data from the low energy neutrino beam facility like JSNS2 experiment, we investigated the angular distribution of outgoing lepton. They show interesting characteristics. The outgoing muon by the KDAR neutrino displayed the forward scattering by the 1^\pm and 2^\pm transitions, although each multipole transition shows different angle dependence. But with the decrease of the incident energy, the peak positions shift more or less to backward direction. But the results by electro-neutrino shows mostly backward scattering patterns. The difference between backward and forward scattering cross sections amount to by almost a factor 2. This different behaviour stems from the outgoing lepton mass. The heavier muon mass scatters forward direction compared to the electron scattered mainly to backward direction.

Finally, we address that this angle dependence of the outgoing leptons may affect the recoil of the target nuclei and can be realized in the forthcoming experiments.

Acknowledgements

This work was supported by the National Research Foundation of Korea (NRF) grant funded by the Korea government (NRF-2021R1A6A1A03043957, NRF-

- [1] W. L. Freedman and M. S. Turner, *Rev. Mod. Phys.* **75**, 1433 (2003).
- [2] J. S. O'Connell, T. W. Donnelly and J. D. Walecka, *Phys. Rev. C* **6**, 719 (1972).
- [3] T. Suzuki, S. Chiba, T. Yoshida, T. Kajino and T. Otsuka, *Phys. Rev. C* **74**, 034307 (2006).
- [4] E. Ydrefors, K. G. Balasi, T. S. Kosmas, J. Suhonen, *Nucl. Phys. A* **866** (2011) 67, Erratum-
ibid. **A 878** (2012) 1.
- [5] K. G. Balasi, E. Ydrefors, T.S. Kosmas, *Nucl. Phys. A* **868** (2011) 82.
- [6] V. Tsakstara, T. S. Kosmas, J. Wambach, *Prog. Part. Nucl. Phys.* **66**, 424 (2011).
- [7] C. Volpe, N. Auerbach, G. Colo, T. Suzuki, and N. Van Giai, *Phys. Rev. C* **62** 015501 (2000).
- [8] S. E. Woosley, D. H. Hartmann, R. D. Hoffmann and W. C. Haxton, *Astrophys. J.* **356**, 272 (1990).
- [9] T. Yoshida, T. Suzuki, T. Chiba, T. Kajino, H. Yokomukura, K. Kimura, A. Takamura and H. Hartmann, *Astrophys. J.* **686**, 448 (2008).
- [10] M. Kusakabe, M.-K. Cheoun, K. S. Kim, M.-a. Hashimoto, M. Ono, K. Nomoto, T. Suzuki, T. Kajino, and G. J. Mathews, Supernova neutrino process of Li and B revisited, *Astrophys. J.* **872**, 164 (2019).
- [11] Heamin Ko, Dukjae Jang, Myung-Ki Cheoun, Motohiko Kusakabe, Hirokazu Sasaki, Xingqun Yao, Toshitaka Kajino, Takehito Hayakawa, Masaomi Ono, Toshihiko Kawano, and Grant J. Mathews, Comprehensive Analysis of the Neutrino Process in Core-collapsing Supernovae, *Astrophys. J.* **937**, 116 (2022).
- [12] T. Suzuki, M. Honma, K. Higashiyama, T. Yoshida, T. Kajino, T. Otsuka, H. Umeda and K. Nomoto, *Phys. Rev. C* **79**, 061603 (2009).
- [13] A. Heger, E. Kolbe, W. C. Haxton, K. Langanke, G. Martinez-Pinedo and S. E. Woosley, *Phys. Lett. B* **606** 258 (2005).
- [14] S. Wanajo, *Astrophys. J.* **647**, 1323 (2006).
- [15] Myung-Ki Cheoun, Eunja Ha, T. Hayakawa, S. Chiba and T. Kajino, *Phys. Rev. C* **82**, 035504, (2010).
- [16] Myung-Ki Cheoun, Eunja Ha and T. Kajino, *Phys. Rev. C* **83**, 028801, (2011).

- [17] L. Alvarez-Ruso *et al.* (NuSTEC Collaboration), *Prog. Part. Nucl. Phys.* **100**, 1 (2018).
- [18] Y. Hino, S. Ajimura, M. K. Cheoun, J. H. Choi, T. Dodo *et al.*, *Eur. Phys. J. C* **82**, 331 (2022).
- [19] S. Ajimura, M. Botran, J. H. Choi, J. W. Choi, M. K. Cheoun, T. Dodo *et al.*, *Nucl. Instrum. Meth. A* **1014**, 165742 (2021).
- [20] C. Athanasopoulos *et al.* (LSND Collaboration), *Phys. Rev. C* **55** 2078 (1997)
- [21] B. E. Bodmann *et al.* (KARMEN Collaboration), *Phys. Lett. B* **332** 251 (1994)
- [22] R. Maschuw, *Prog. Part. Nucl. Phys.* **40** 183, (1998)
- [23] B. A. Armbruster *et al.* (KARMEN Collaboration), *Phys. Lett. B* **423** 15 (1998)
- [24] A. Aguilar-Arevalo *et al.* (LSND), *Phys. Rev. D* **64**, 112007 (2001), arXiv:hep-ex/0104049 [hep-ex].
- [25] A. A. Aguilar-Arevalo *et al.* (MiniBooNE Collaboration), *Phys. Rev. Lett.* **120**, 141802 (2018).
- [26] M. Harada *et al.* (JSNS2 Collaboration), arXiv:1310.1437 (2013).
- [27] M. Elnimr *et al.*, The OscSNS White Paper, in Proceedings of the 2013 Community Summer Study on the Future of U.S. Particle Physics: Snowmass on the Mississippi (CSS13), Report No. FERMILAB-CONF-13-648 and SLAC-PUB-15960 (2013), arXiv:1307.7097.
- [28] A. A. Aguilar-Arevalo *et al.*, *Phys. Rev. D* **106**, No. 1 (2022).
- [29] K. Scholberg *et al.* (COHERENT Collaboration), Inelastic Neutrino-Nucleus Interaction Measurements with COHERENT, Snowmass LOI-139, 2020 (unpublished).
- [30] D. Akimov, *et al.*, *Science*, **357**, 1123 (2017).
- [31] J. R. Distel, B. T. Cleveland, K. Lande, C. K. Lee, P. S. Wildenhain, G. E. Allen, and R. L. Burman, *Phys. Rev. C* **68**, 054613 (2003).
- [32] K. S. Kim and Myung-Ki Cheoun, *Phys. Lett. B* **679**, 330 (2009).
- [33] A. Nikolakopoulos, V. Pandey, J. Spitz, and N. Jachowicz, *Phys. Rev. C* **103**, 064603 (2021).
- [34] Myung-Ki Cheoun, Eunja Ha, K. S. Kim and T. Kajino, *J. of Phys. G* **37**, 055101, (2010).
- [35] Myung-Ki Cheoun, Eunja Ha, S. Y. Lee, W. So, K. S. Kim and T. Kajino, *Phys. Rev. C* **81**, 028501 (2010).
- [36] T. W. Donnelly and W. C. Haxton, *ATOMIC DATA AND NUCLEAR DATA* **23**, 103 (1979).
- [37] J. D. Walecka, *Muon Physics*, edited by V. H. Hughes and C. S. Wu (Academic, New York, 1975), Vol II.
- [38] J. S. O'Connell, T. W. Donnelly, and J. D. Walecka, *Phys. Rev. C* **6**, 719 (1972).

- [39] M. K. Cheoun, A. Bobyk, Amand Faessler, F. Simcovic and G. Teneva, Nucl. Phys. **A 561**, 74 (1993) ; Nucl. Phys. **A 564**, 329 (1993); M. K. Cheoun, G. Teneva and Amand Faessler, Prog. Part. Nuc. Phys. **32**, 315 (1994) ; M. K. Cheoun, G. Teneva and Amand Faessler, Nucl. Phys. **A 587**, 301 (1995).
- [40] A. Bortrungo and G. Colo, Eur. Phys. J. **A24 S1**, 109, (2005).
- [41] Giampaolo Colo, Acta Physica Polonica **B 37**, 2235, (2006).
- [42] Jonathan Angel, Phys. Rev. **C 57**, 2004 (1998).
Otsuka, Phys. Rev. **C 74**, 034307 (2006).
- [43] N. Paar, D. Vretenar, T. Marketin, and P. Ring, Phys. Rev. **C 77**, 024608 (2008).
- [44] E. Kolbe, K. Langanke, G. Martinez-Pinedo, Phys. Rev. **C 60**, 052801 (1999).
- [45] E. Kolbe, K. Langanke, G. Martinez-Pinedo and P. Vogel, J. Phys. **G 29**, 2569 (2003).
- [46] J. D. Walecka, Ann. Phys. (NY) **83**, **491** (1974).
- [47] C. J. Horowitz and B. D. Serot, Nucl. Phys. **A 368**, 503 (1981).
- [48] J. Boguta and A. R. Bodmer, Nucl. Phys. **A 292**, 413 (1977).
- [49] A. Bouyssy, S. Marcos, and P. Van Thieu, Nucl. Phys. **A 422**, 541 (1984).
- [50] Y. K. Gambhir, P. Ring, and A. Thimet, Ann. Phys. (NY) **198**, 132 (1990).
- [51] P. A. M. Guichon, Phys. Lett. **B 200**, 235 (1988).
- [52] K. Saito and A. W. Thomas, Phys. Lett. **B 327**, 9 (1994); K. Saito, K. Tsushima, and A. W. Thomas, Nucl. Phys. **A 609**, 339 (1996); Phys. Rev. **C 55**, 2637 (1997).
- [53] S. Nagai, T. Miyatsu, K. Saito, and K. Tsushima, Phys. Lett. **B 666**, 239 (2008).
- [54] T. Miyatsu, M. K. Cheoun, and K. Saito, Phys. Lett. **B 709**, 242 (2012); Astrophys. J. **813**, 135 (2015).
- [55] Tsuyoshi Miyatsu, Myung-Ki Cheoun, Kyungsik Kim, Koichi Saito, Phys. Lett. **B 843**, 138013 (2023).
- [56] Tsuyoshi Miyatsu, Myung-Ki Cheoun, Koichi Saito, Astrophys. J. **929**, 82 (2022).
- [57] S. Choi, T. Miyatsu, Y. Kwon, K. Kim, M.-K. Cheoun, and K. Saito, Phys. Rev. **C 104**, 014322 (2021).
- [58] K. S. Kim, S. Choi, M.-K. Cheoun, and H. Kim, Phys. Rev. **C 105**, 024606 (2022).
- [59] Kyungsik Kim, Hana Gil, Chang Ho Hyun, Phys. Lett. **B 833**, 137273 (2022).
- [60] K. S. Kim, Soonchul Choi, Tsuyoshi Miyatsu, Myung-Ki Cheoun, Hungchong Kim, Phys. Rev. **C 107**, 024607 (2023).

- [61] M. Bhattacharya, C. D. Goodman, and A. Garcia, Phys. Rev. **C 80**, 055501 (2009).
- [62] Brian D. Serot, John Dirk Walecka, Adv. Nucl. Phys. **16**, 1 (1986).
- [63] F. Akbar, M. Sajjad Athar and S. K. Singh, J. Phys. G: Nucl. Part. Phys. **44**, 125108 (2017).